Proceedings of the ASME 2020
14th International Conference on Energy Sustainability
ES2020
June 8-10, 2020, Denver, CO, USA

SAND2019-15228C

DRAFT

ES2020-12356

# IMPROVING NEXT-GENERATION FALLING PARTICLE RECEIVER DESIGNS SUBJECT TO ANTICIPATED OPERATING CONDITIONS

**Brantley Mills, Reid Shaeffer, Lindsey Yue, and Clifford K. Ho**
Sandia National Laboratories
Albuquerque, New Mexico, 87185-0836, USA
bramill@sandia.gov

## ABSTRACT

*The thermal performance of a candidate next-generation falling particle receiver (FPR) is analyzed subject to various expected operating conditions. This receiver design was created from the result of an extensive optimization study and developed to support the Generation 3 Particle Pilot Plant (G3P3). Previous analysis had demonstrated high thermal efficiencies for the receiver at nominal quiescent conditions, but further analysis was required to demonstrate that the receiver could maintain that thermal performance in all anticipated environments. In this study, the thermal efficiency was numerically evaluated using a CFD model for different wind conditions and shown to maintain a thermal efficiency above 83%. Moreover, the anticipated design power from the heliostats was shown to not exceed maximum temperature limits of the wall materials as a result of spillage. Additional features were numerically explored including the addition of a chimney to capture particle fines and waste heat and multi-stage concept to maximize curtain opacity. Particle fines of 10 µm were shown to be captured by the inclusion of this chimney, and the multi-stage design decreased radiative losses and minimized wall temperatures behind the particle curtain.*

Keywords: concentrating solar power, falling particle, receiver, thermal efficiency, wind, simulation.

## 1. INTRODUCTION

Particle-based concentrating solar power plants are a viable option to help meet future baseload electricity demands [1,2]. The use of particles over a more traditional heat transfer fluids (*e.g.* water, salts, etc.) offers a number of advantages including: the ability to reach very high temperatures resulting in higher solar-to-electric efficiency, the ability to directly store energy as sensible energy, and the absence of flux limitations in the receiver piping typically used to contain the heat transfer fluid. In particular, this last advantage enables smaller receivers with fewer losses (both radiatively and convectively to the environment) and higher thermal efficiencies. Furthermore, particles are an inexpensive and commercially available medium without an upper temperature limit that do not require trace heating.

An essential component of a particle-based concentrating solar power plant is the particle receiver. Falling particle receivers (FPRs) are a proven design that have been experimentally shown to reach particle outlet temperatures in excess of 700°C [3]. In a FPR, particles are released in a curtain and fall with gravity past a beam on concentrated sunlight. The majority of FPR designs have been cavity-type receivers that help to minimize radiatively losses to the environment and the effects of wind on the particles [4,5,6]. Some designs have featured obstructions or a multi-stage concept to slow the particles as they fall through the receiver cavity maximizing both the residence time and the curtain opacity [7,8].

As part of the Generation 3 Particle Pilot Plant (G3P3) project, a next-generation 1 $MW_{th}$ particle receiver is being designed with a targeted thermal efficiency approaching 90% utilizing the National Solar Thermal Test Facility (NSTTF) heliostat field. Design of the particle receiver is adhering to the following strategy: (1) optimization of a candidate geometry under quiescent conditions, (2) investigation of candidate geometry performance subject to wind, and (3) investigation of maximum temperatures when irradiated with the NSTTF heliostat field. Additionally, two features are being investigated as further improvements to the design: (1) a 'chimney' to capture advective and particle losses from the aperture and (2) a multi-stage concept.

A thorough optimization routine has been previously performed to define a candidate geometry for the G3P3 particle receiver [9]. This falling particle receiver (FPR) design features a north-facing cavity recessed into the tower through a converging tunnel. Coupled CFD models of the candidate receiver have demonstrated that a thermal efficiency of 87% can

be achieved in quiescent conditions; however, further investigation is ongoing to ensure that the particle receiver can adequately sustain comparable thermal efficiencies at all operating conditions and enable steady-state operation when subjected to the designed irradiance from the NSTTF heliostats.

In this paper, CFD models of the candidate receiver are used to assess the thermal efficiency subject to various detrimental wind speeds and directions. Earlier studies have suggested that more northern winds were the most detrimental to a north-facing cavity-type FPR [10]. Ray tracing models developed are also used in conjunction with CFD models to ascertain the maximum temperatures of the spillage board and receiver tunnel subject to the irradiance provided by the NSTTF field. Additional numerical studies are also performed including other receiver features to further improve the design. Visualization of the entrained air in the cavity at temperature revealed that the presence of a chimney near the exit of the receiver tunnel can be used to capture advective losses and escaping particle fines. Finally, the integration of a multi-stage concept is evaluated to determine the concept's effect on the thermal performance and the maximum receiver temperatures.

The remainder of this paper is organized as follows. First, the computational models used to investigate these scenarios are described. These include a CFD model of the conceptual receiver design and a ray-tracing model of the receiver and NSTTF heliostat field. Then, the receiver is evaluated for different wind directions and speed to determine the effect on the thermal efficiency. Next, ray tracing models are used to evaluate the maximum irradiance expected on spillage boards and nominal conditions are compared to values in the CFD model to correlate with expected maximum operating temperatures. Next, CFD models of the receiver design integrated with a chimney are evaluated. Finally, the receiver design is integrated with a multi-stage concept to ascertain the effect it has on the efficiency and temperature inside the receiver.

## 2. COMPUTATIONAL MODELS

### 2.1 Computational Fluid Dynamics Model

The CFD model used in this analysis was developed in ANSYS Fluent® 19.2 using a Lagrangian/Eulerian modeling approach that has been discussed previously in the literature [11,12]. A description of this model is provided here and the initial optimized geometry from Reference 9 is shown in Figure 1. The geometry features a north-facing cavity recessed into the tower by a converging tunnel referred to as the Solar Nod Optimized Unobstructing Tunnel (SNOUT).

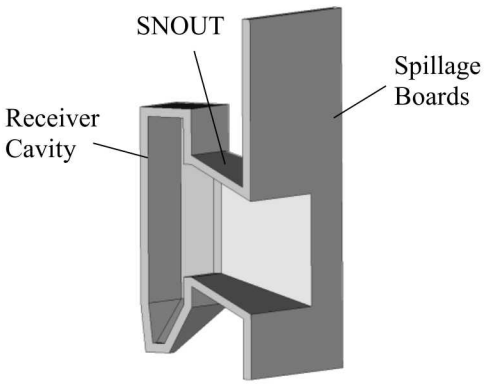


Figure 1. Solid model of the optimized FPR [9] cut along the midplane

Lagrangian particle parcels are released from the top of the receiver cavity and fall through the domain via gravity past a beam of concerted sunlight. The particles are coupled to the air continuum inside and outside of the receiver via drag forces, heat transfer, and turbulent interactions. A two-equation turbulence model, the realizable k–ε model [13], was applied to model turbulence in the air domain and Fluent's "scalable" wall functions were applied to model turbulent wall interactions to be more robust with varying mesh sizes at the fluid–wall boundaries. To simplify the computation expense, only the air in front of the spillage board is included outside of the receiver cavity. That is, an infinite spillage board is assumed. Conduction was modeled through the alumina silica fiberboard walls assuming 10.2 cm of thickness in all locations. Behind the spillage board, convection and radiation to the ambient environment was included assuming a natural convection coefficient of 10 $W/m^2K$.

Particles were modeled as CARBO HSP 40/70 with nominal particle diameters of 350 μm. CARBO HSP 20/40 particles have also been used at the NSSTF with larger diameters approaching 700 μm, and the properties for these particles were used here as a surrogate and taken from References [12,1412]. Particle collisions with the walls were model as perfectly elastic except in the hopper where the are removed from the domain once they contact a surface. This assumes that effects from particles bouncing the hopper are negligible to further minimize the computational expense. Particle-to-particle collisions are also neglected under the assumption that the volume fraction of particles in the curtain is small. This assumption has been shown to be valid for volume fractions less then 10% and FPRs at this scale have been shown to have volume fractions less than 10% for most of the fall distance [15].

A non-grey discrete ordinates (DO) radiation model is used to model radiative transport in the receiver. The purpose of the non-grey model was to capture the thermal emissions from the receiver walls and particles at a higher wavelength than the incoming solar irradiation from the field. The non-grey model was divided into three bands: 0.1< 2.5 μm, 2.5-4.5 μm, and 4.5 > 100 μm. All incident solar irradiation enters the domain at the smallest wavelength. The delineation in the thermal emissions at 4.5 μm accounts for differences in radiative properties for the alumina silica fiberboard walls.

Solar radiation entering the computational domain is defined based on the NSTTF heliostat field accounting for the expected G3P3 receiver location relative to the field. Using NREL's ray-tracing software, SolTrace [16], a simulation is performed for the irradiation BC at solar noon on the equinox. The radiation intensity and directionality from the heliostat field on a plane 3 m in front of the cavity aperture is computed for a minimum of 10 million ray intersections. For a 25x25 unit grid on that plane, the rays crossing that plane were locally averaged. Then the resulting vectors were averaged and fit with analytical expressions to create functions that could easily be implemented into Fluent via a user defined function (UDF). These functions described the intensity, direction, and beam spread variation across that plane for the DO model.

The mesh size for this modeling approach has been previously studied in the literature to assure appropriate spatial discretization inside the receiver cavity (References 9-11). In each simulation, the number of cells varies depending on the particular feature or conditions being simulated. However, guidance from these previous works is used to ensure convergence in the solution for decreasing cell size.

### 2.2 Ray-Tracing Model

As described above, NREL's SolTrace v3.1 is used to simulate the radiative transport to the receiver from the NSTTF heliostat field. The model is based upon previously used models of the NSTTF field that has been described in the literature [17]. Additional surfaces are included to represent the spillage board and SNOUT at the tentative aperture centroid location: 40.5 m West, 8.5 m North, and 41.837 m up from the base of the existing tower's center. Note that this receiver is not a truly north-facing receiver design since it will be angled to face the heliostat field centroid from an offset position.

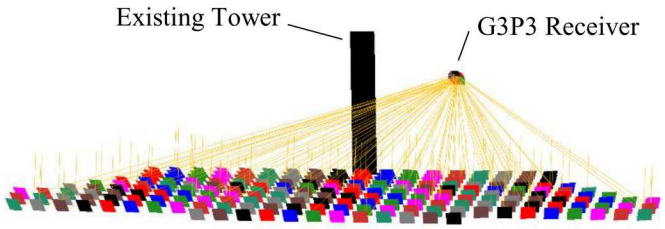


Figure 2. Visualization of irradiation from the NSTTF field to the G3P3 receiver using the ray tracing model

The NSTTF heliostat field includes up to 216 heliostats and are modeled with a reflectivity, slope error, and specularity error of 0.885, 1.2 mrad, and 0.05 mrad, respectively. The SNOUT and spillage board surfaces are modeled as opaque with a reflectivity of 0.2, and multiple hits are allowed for each ray. Optical errors are included as well as a custom sun shape profile including available optical errors as depicted in Figure 3. For the simulations provided in this paper, up to $1\times10^7$ ray intersections are generated for each case, and a DNI of 1000 W/m$^2$ is assumed.

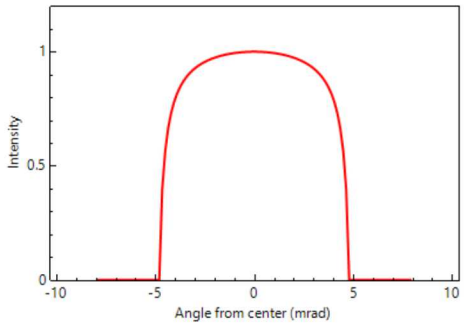


Figure 3. Sun shape profile used in the ray-tracing model.

## 3. PARAMETRIC WIND STUDY

To determine the effect of various wind conditions on the optimized G3P3 candidate geometry, a parametric study of various detrimental wind conditions is performed on the design. As discussed in Reference 10, more northern wind directions were shown to be the most detrimental to FPR performance. As such, the performance of the receiver is evaluated for wind directions of N, NW, and NNW at wind speeds of 0, 5, 10, and 15 m/s. Incident power to the receiver is evaluated near the maximum anticipated power, $Q_{max}$, provided by the NSTTF field at 2.5 MW. Particle inlet temperatures to the receiver, $T_{i,p}$, are modeled at 575°C with a particle mass flow rate, $\dot{m}_p$, of 9.5 kg/s. At the time of this analysis, these represented approximately nominal conditions for the G3P3 receiver. Recall from Figure 2 that this receiver is not pointing directly north to accommodate the NSTTF heliostat field. However, for simplicity wind directions will be reported as if the receiver were truly north-facing.

The thermal efficiency of the receiver is used as the primary metric to evaluate the effect of the wind on the receiver. The thermal efficiency is defined as:

$$\eta_{th} = \frac{Q_a}{Q_i} = \frac{\dot{m}_p(h_{o,p} - h_{i,p})}{Q_i} = \frac{\dot{m}_p \int_{T_{i,p}}^{T_{o,p}} c_P(T)dT}{Q_i} \quad (1)$$

where $Q_a$ is the absorbed thermal power in the particles, $Q_i$ is the incident thermal radiative power, $h_p$ is the enthalpy of the particles, and $c_P(T)$ is the specific heat of the particles (J/kg·K) as a function of temperature defined as:

$$c_P(T) = 365 \cdot T_p^{\,0.18} \quad (2)$$

where the mean particle temperature is in ºC between 50ºC $\leq T \leq$ 1100ºC [12].

The thermal efficiency of the receiver is plotted versus various wind speeds for the three different wind directions and quiescent conditions in Figure 4a. A plot of the air velocity vectors colored by temperature looking down at a horizontal plane at the middle of the aperture is also included in Figure 4b for a NW, 15 m/s wind (the worst case depicted in Figure 4a). These plots reveal the effect that the SNOUT has on incoming northern winds by helping to create a recirculation in front of the aperture minimizing cold air entering the receiver cavity. This flow field is fundamentally different from the flow created under quiescent conditions but does not result in a significant increase

in hot air escaping the receiver. Note that hot air escaping the receiver cavity is ultimately replaced by cold air cooling the particles and is referred to in this paper as an advective loss. Advective losses can contribute significantly to a decreased receiver thermal efficiency. For the case depicted in Figure 4b, the receiver efficiency remains above 83% suggesting adequate performance in the worst expected wind conditions.

Finally, note that this study was performed on the original optimized geometry of the G3P3 receiver. This study will ultimately need will need to be repeated as the design continues to evolve and reaches its final iteration. Future work also includes simulating the receiver in the tower to more accurately capture the effects of wind from other directions.

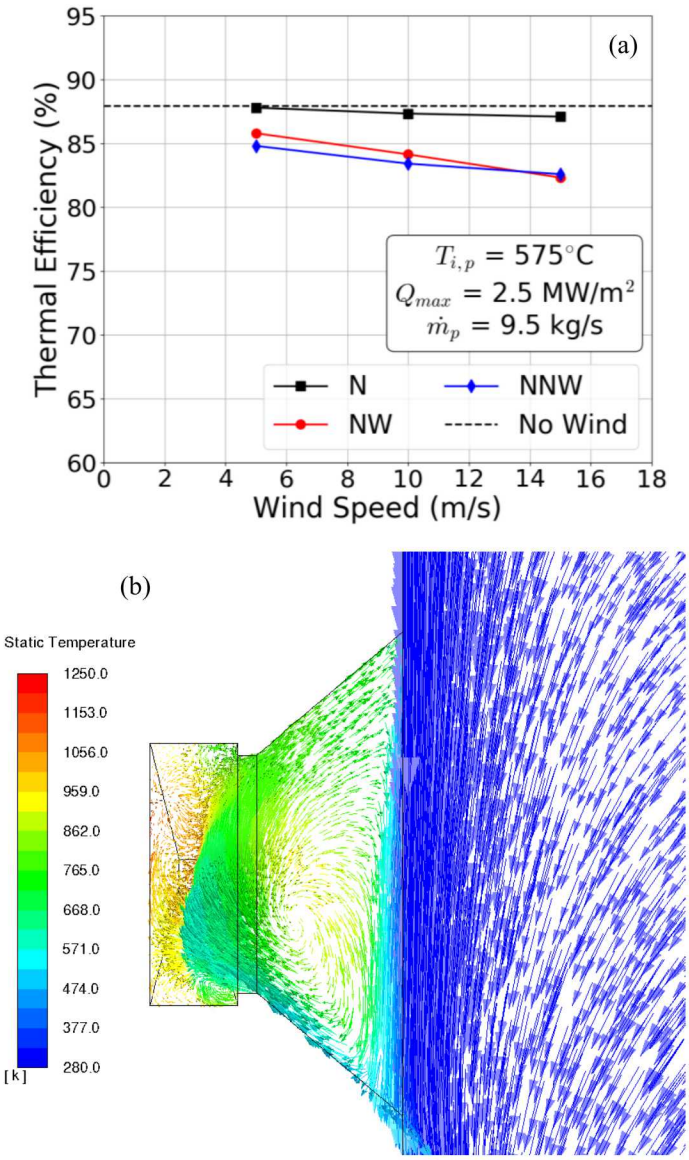


Figure 4. Receiver thermal efficiency plotted versus wind speed for various wind directions (a) and a plot of velocity vectors colored by air temperature at a horizontal midplane of the aperture for a 15 m/s NW wind (b)

## 4. SPILLAGE ON THE RECEIVER

Preliminary results from the ray-tracing model revealed early modifications to the receiver were necessary to accommodate the NSTTF heliostat field. First, the east and west surfaces of the SNOUT require widening to ensure that the horizontal acceptance angle is sufficient given that the receiver is offset from the original solar tower. Therefore, the acceptance angle is increased from 84° to 112°. Furthermore, early results indicated that the top leading edge of the SNOUT and the bottom spillage board were receiving too much incident flux from spillage. As a result, the top leading edge is truncated 0.25 m into the SNOUT and the bottom SNOUT surface angle is increased by 10 degrees from the horizontal.

With these changes, the peak and average incident fluxes (MW/m$^2$) with total incident power to the receiver aperture (MW) for a 1.5 m$^2$ aperture are computed at the summer solstice, the winter solstice, and the equinox at -3, 0 and +3 hours from solar noon. The results are summarized in Table 1. For each case, the uncertainty in the peak and average fluxes is less than 2.0% and 0.3%, respectively. As shown in the table (time is listed as hours from solar noon), an average power to the receiver aperture of at least 1.85 MW is feasible throughout the year. Note that the off-center location of the G3P3 receiver provides higher power to the receiver in the afternoon than in the morning. One additional advantage of the SNOUT is that it also provides additional power to the receiver cavity from reflections off of the SNOUT surfaces. However, this comes at a cost of lower survivable incident fluxes than traditional typical spillage boards from decreased viewfactors when reradiating to the ambient environment.

Table 1. Maximum flux and power to the G3P3 receiver

| | Time | Peak Flux (MW/m$^2$) | Avg. Flux (MW/m$^2$) | Total Power (MW) |
|---|---|---|---|---|
| Equinox | -3 | 2.30 | 1.54 | 2.31 |
| | 0 | 3.14 | 1.95 | 2.93 |
| | 3 | 2.76 | 1.76 | 2.64 |
| Summer Solstice | -3 | 1.70 | 1.23 | 1.85 |
| | 0 | 2.57 | 1.68 | 2.52 |
| | 3 | 2.20 | 1.50 | 2.25 |
| Winter Solstice | -3 | 2.46 | 1.54 | 2.31 |
| | 0 | 3.20 | 1.99 | 2.99 |
| | 3 | 2.92 | 1.82 | 2.73 |

Given that the NSTTF field is not designed for the G3P3 receiver, some heliostats do not have ideal positions with the anticipated receiver location. However, the field generally provides more power than is needed for the G3P3, so several heliostats can be selectively excluded from the field to provide a more optimized beam that minimizes spillage on the SNOUT and surrounding spillage boards. Using the ray-tracing model, the irradiances at high flux locations are evaluated subject to a beam providing 2 MW to the aperture on the equinox at solar noon. To deliver 2 MW to the receiver, heliostats are iteratively excluded from the field to minimize spillage. The irradiances on the East SNOUT wall, the West SNOUT wall, the truncated top SNOUT wall, and the bottom spillage board below the SNOUT

are plotted in Figure 5. As shown in the figure, irradiances of up to 0.81 MW/m$^2$ are expected in these locations at these conditions.

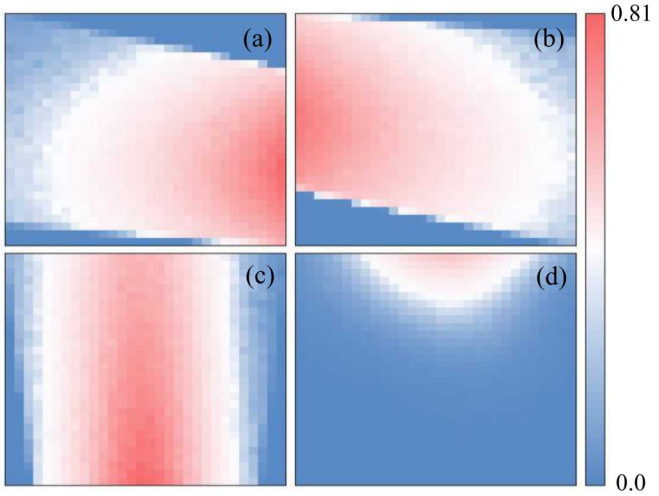


Figure 5. Plots of irradiance from the ray-tracing model (in MW/m$^2$) for the East SNOUT wall (a), West SNOUT wall (b), truncated top SNOUT wall (c), and the bottom spillage board (d)

The CFD model can be used to determine the temperature of a spillage board subject to a given irradiance. These surfaces will experience convection, reflection, and re-radiation to the environment that offsets some of the incident flux. Recall that the CFD model is using a DO model to capture radiation transport from a surface 3 m in front of the receiver aperture. Therefore, irradiances on the receiver walls will not be equivalent to those modeled from ray-tracing model particularly near the periphery of the beam. However, for regions with equivalent irradiances and similar locations on the spillage boards, the temperatures should be comparable. A contour plot of the temperatures on the SNOUT walls and spillage board is depicted in Figure 6 for a 2 MW beam to the receiver at solar noon on the equinox. For various irradiances, the temperature range on the spillage boards and SNOUT surface are summarized in Table 2. As shown in the table for irradiances of up to 0.9 MW/m$^2$, temperatures on the surface are expected to be less than ~1570°C. For alumina silica fiberboard walls, the maximum temperature of the material is ~1760°C [12] suggesting that the boards can survive in steady-state operation for receiver power up to 2 MW.

Table 2. Wall temperatures at various irradiances from the CFD model

| Irradiance Range (MW/m$^2$) | Temperature Range (°C) |
|---|---|
| 1.1 – 1.2 | 1551.6 – 1694.7 |
| 1.0 – 1.1 | 1501.9 – 1656.3 |
| 0.9 – 1.0 | 1447.1 – 1616.3 |
| **0.8 – 0.9** | **1387.3 – 1568.5** |
| 0.7 – 0.8 | 1316.9 – 1513.0 |
| 0.6 – 0.7 | 1238.7 – 1449.6 |

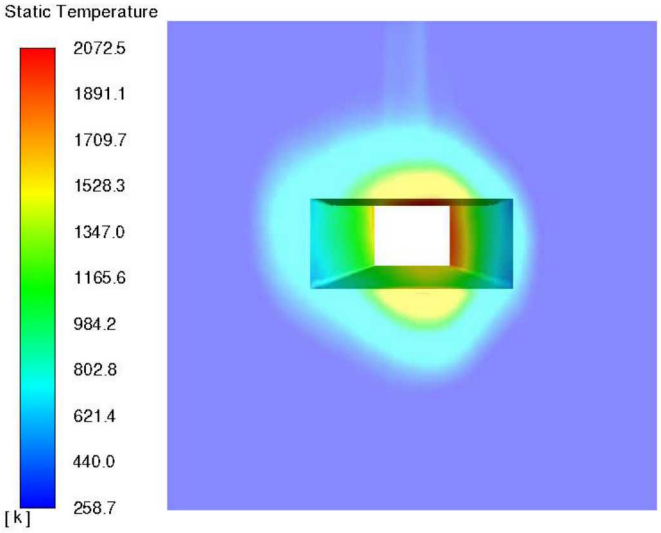


Figure 6. Temperature on the SNOUT surfaces and spillage boards (K) from the CFD model on the equinox at solar noon. Using all NSTTF heliostats.

## 5. EFFECT OF A CHIMNEY

One of the benefits observed in the G3P3 optimization reported in Reference 10, was a favorable flow field that inhibited advective losses from the receiver. In the preceding parametric wind study, that flow is also observed for quiescent conditions and is depicted for reference in Figure 7. Effectively, entrained air is redirected to inhibit cold air ingress at the bottom of the receiver aperture and impinge on the upper SNOUT surface returning a large fraction of heated air back into the receiver cavity. Some heated air does escape the receiver along the top surface of the SNOUT, which presents an opportunity to re-capture this air and any particle fines trapped in it.

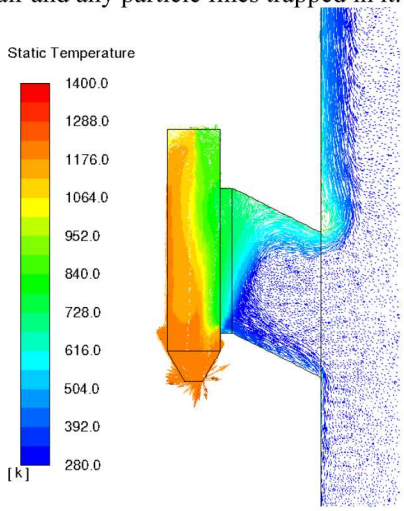


Figure 7. Air velocity vectors colored by temperature (K) along the midplane from the parametric wind study for quiescent conditions.

A ‘chimney’ is a proposed feature that can be integrated with the existing SNOUT. The proposed chimney is depicted in Figure 8. It is assumed that downstream disruptions to the flow in the SNOUT would not adversely affect the performance and

provide two additional benefits: the ability to recover losses from the receiver and the ability to capture and filter particle fines leaving the aperture. With regards to particle fines, particle diameters between 1–10 µm are generally the sizes of interest as they pose the greatest inhalation risk to people [**CITE**]. However, particle diameters of that size are also sensitive to the flow field and can be redirected up the chimney before leaving the spillage board plane.

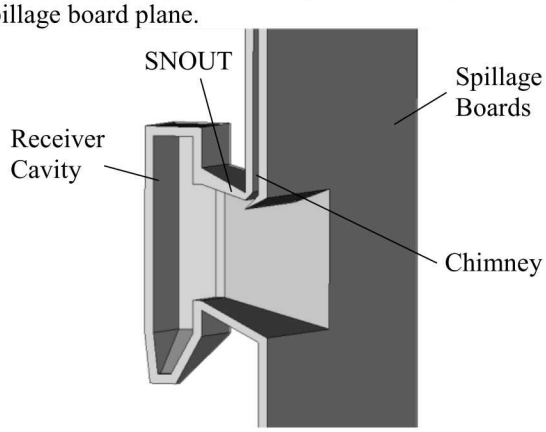


Figure 8. G3P3 receiver integrated with the proposed chimney in the SNOUT cut along the midplane

A nominal CFD simulation is performed on the G3P3 receiver integrated with a chimney. Other features described in the previous section to accommodate the NSTTF heliostat field are also integrated in the receiver design. The chimney surface is modeled as an open pressure boundary condition at ambient conditions. The receiver is simulated for an incident power of 2 MW on the equinox at solar noon. A particle mass flow rate of 8 kg/s is assumed with particles entering the receiver at 615°C. Velocity vectors colored by the air temperature are plotted along the midplane of the receiver in Figure 9a demonstrating that much of the hot air leaving the receiver is being directed up the chimney. For this case, the receiver efficiency is predicted to be 85.8% with advective losses of 4.1%, radiative losses of 9.8% (6.1%, 1.7%, and 2.0% for the three radiation bands from smallest to largest wavelengths, respectively) and 0.4% for losses through the walls. In Figure 9b, traces of particle fines at 10 µm dimeters are depicted demonstrating the all of the particles are also going up the chimney.

It should be emphasized that for the chimney to function as simulated above, it must remain partially open to the atmosphere. That is, any particle filtration must not significantly obstruct the flow of hot air up the chimney (*i.e.* filters across the chimney's cross section will likely obstruct the flow). Designs to filter the particle files without obstructing flow are presently under consideration but are left here as future work. Furthermore, the effect of the chimney subject to external wind is also left as future work.

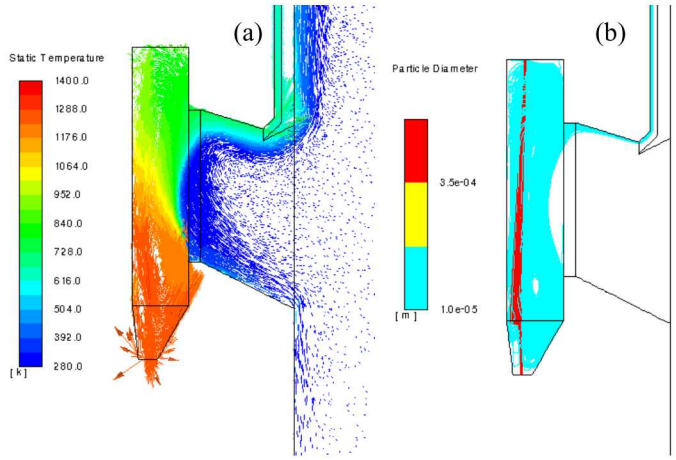


Figure 9. Air velocity vectors colored by temperature (K) along the midplane (a) and the traces for particles with diameters of 10 µm (b)

## 6. MULTI-STAGE DESIGN

The last feature considered for the G3P3 receiver is the implementation of a multi-stage design. For this feature the back wall of the receiver is sloped, and two staggered troughs are integrated with the back wall in the paths of the falling particles. At each trough, the particles accumulate and spill over the front edge slowing the particles as they fall through the receiver without exposing any surface directly to irradiation from the heliostat field. This effect increases the particle curtain opacity compared to a completely free-fall design. This concept has been described in the literature in other forms [8] and is described as the staggered angle iron receiver (StAIR) concept. Of particular interest for this design is the receiver efficiency and back wall temperatures behind the particle curtain.

To model this concept in the existing CFD model, several assumptions are made to make the problem more computationally tractable. First, the geometry of the troughs are simplified such that each level is represented as a simple angled surface with special particle-interaction properties. The geometry of the receiver is depicted in Figure 10. When a particle impacts a trough surface (representative of a trough full of particles), the particle velocity is reset and given a forward rebound velocity (in this case, 0.3 m/s) that closely matches empirical observations of small scale testing of the multi-stage concept. This approach is described in more detail in Reference 18. Although this is not a first-principles based approach, it approximately captures the varying curtain opacity through the height of the receiver in steady-state conditions enabling predictions for the receiver thermal efficiency using the same Lagrangian-Eulerian modeling approach.

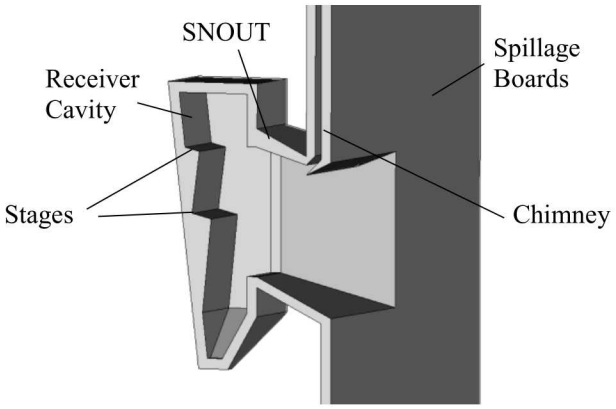


Figure 10. G3P3 receiver integrated with a multi-stage release design cut along the midplane

This receiver is again simulated for an incident power of 2 MW on the equinox at solar noon. A particle mass flow rate of 8 kg/s is assumed with particles entering the receiver at 615°C. As before, a chimney is also included in the design to enable comparisons with and without the multi-stage feature. Velocity vectors colored by the air temperature are plotted along the midplane of the receiver in Figure 11a demonstrating a similar beneficial flow field as observed previously. The particle temperatures across the curtain are also shown in Figure 11b. For this case, the receiver efficiency is predicted to be 87.9% with advective losses of 4.3%, radiative losses of 7.4% (3.9%, 1.7%, and 1.8% for the three radiation bands from smallest to largest wavelengths, respectively) and 0.3% for losses through the walls. As expected, radiative losses decreased by 2.4% from the previous simulation due the increased curtain opacity. This is observed primarily in the smallest wavelength band that are more closely associated with reflected radiative losses. Some of this improvement in radiative losses is offset by a small increase in advective losses.

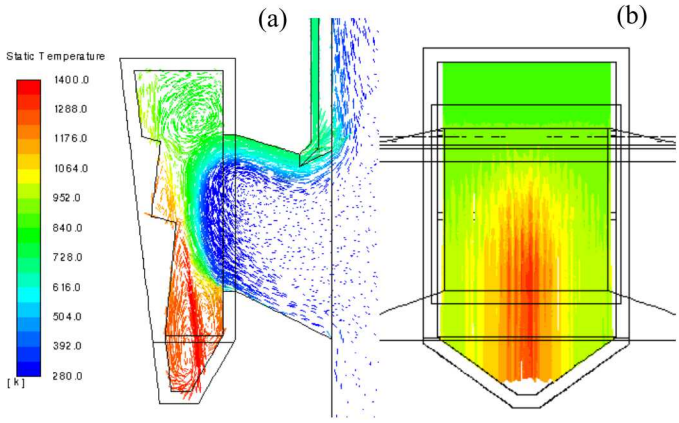


Figure 11. Air velocity vectors colored by temperature (K) along the midplane (a) and the traces for particles colored by temperature (K) (b)

In addition to decreased radiative losses, the temperature of the back wall behind the particle curtain decreases significantly. In the free-fall design, back wall temperatures reach a maximum of 1613°C, whereas in the multi-stage design, back wall temperatures only reached a maximum of 1373°C. As before, this improvement in back wall temperature is a result of increased curtain opacity.

## 7. CONCLUSIONS

In support of the Generation 3 Particle Pilot Plant project, a candidate next-generation falling particle receiver has been developed from an extensive optimization study. This receiver has been shown to have promising thermal efficiencies of 86.9% for quiescent conditions, but additional study was required to demonstrate that the receiver design still maintains high thermal performance at all anticipated operating conditions. In this study, the thermal performance of the receiver was evaluated under various detrimental wind conditions and subject to expected irradiances from the NSTTF heliostat field. In addition, the thermal performance of two additional features, a chimney and a multi-stage release, was also evaluated.

For various detrimental wind directions and wind speeds, the thermal efficiency of the receiver was shown to be greater than 83%. In addition, spillage for nominal operating conditions at 2 MW thermal power to the receiver was found to not result in exceeding maximum material temperature limits for the SNOUT and the spillage boards. The inclusion of the chimney did not significantly affect the thermal performance while enabling the capture of particle fines with diameters as small as 10 μm. Finally, when integrated with a multi-stage feature, radiative losses were modestly decreased while wall temperatures behind the particle curtain were reduced by 240°C.

## ACKNOWLEDGEMENTS

This material is based upon work supported by the U.S. Department of Energy's Office of Energy Efficiency and Renewable Energy (EERE) under Solar Energy Technologies Office (SETO) Agreement Number 34211. Sandia National Laboratories is a multi-mission laboratory managed and operated by National Technology and Engineering Solutions of Sandia, LLC., a wholly owned subsidiary of Honeywell International, Inc., for the U.S. Department of Energy's National Nuclear Security Administration under contract DE-NA0003525.

## REFERENCES

[1] Hruby, J. M., Steele, B. R., "A solid particle central receiver for solar energy," *Chemical Engineering Progress*, **82**, 44 (1986).

[2] Ho, C., Christian, J., Gill, D., Moya, A., Jeter, S., Abdel-Khalik, S., Sadowski, D., Siegel, N., Al-Ansary, H., Amsbeck, L., Gobereit, B., Buck, R., "Technology advancements for next generation falling particle receivers," *Proceedings of the SolarPACES 2013 International Conference,* **49** (Energy Procedia), 398 (2014).

[3] Ho, C.K., J.M. Christian, J. Yellowhair, K. Armijo, and S. Jeter, *Performance Evaluation of a High-Temperature Falling Particle Receiver*, in *ASME Power & Energy Conference*, Charlotte, NC, June 26-30, 2016.

[4] Gobereit, B., Amsbeck, L., Buck, R., Pitz-Paul, R., Röger, M., Müller-Steinhagen, H., "Assessment of a falling solid

particle receiver with numerical simulation," *Solar Energy*, **115**, 505 (2015).
[5] Khalsa, S., Christian, J., Kolb, G., Röger, M., Amsbeck, L., Ho, C. K., Siegel, N., Moya, A., "CFD Simulation and Performance Analysis of Alternative Designs for High-Temperature Solid Particle Receivers," *Proceedings of ASME 2011 5th International Conference on Energy Sustainability*, Washington, DC, USA, August 7-10, 2011.
[6] Röger, M., Amsbeck, L., Gobereit, B., Buck, R., "Face-Down Solid Particle Receiver Using Recirculation", *Sournal of Solar Energy Engineering*, **133**, 031009 (2011).
[7] C. K. Ho, et al., On-Sun Testing of an Advanced Falling Particle Receiver System, in SolarPACES 2015 Conference, Cape Town, South Africa, October 13-16, 2016.
[8] Kim, J., Kumar, A., Gardner, W., Lipinski, W., "Numerical and Experimental Investigation of a Novel Multi-Stage Falling Particle Receiver," SolarPACES 2018
[9] Mills, B., Shaeffer, R., Yue, L., Ho, C. K., "Optimizing a Falling Particle Receiver Geometry Using CFD Simulations to Maximize the Thermal Efficiency," SolarPACES 2019
[10] Mills, B., Shaeffer, R., Ho, C. K., Yue, L., "Modeling the Thermal Performance of Falling Particle Receivers Subject to External Wind," *Proceedings of the ASME 2019 13th International Conference on Energy Sustainability*, Bellevue, WA, USA, July 15-17, 2019.
[11] Mills, B., Ho, C. K., "Simulation and Performance Evaluation of On-sun Particle Receiver Tests," Presented at SolarPACES2018, October 2-5, 2018, Casablanca, Morocco.
[12] Ho, C.K., B. Mills, and J.M. Christian, 2016, *Volumetric Particle Receivers for Increased Light Trapping and Heating*, in *ASME Power & Energy Conference*, Charlotte, NC, June 26-30, 2016.
[13] T.-H. Shih, W. W. Liou, A. Shabbir, Z. Yang, and J. Zhu. "A New - Eddy-Viscosity Model for High Reynolds Number Turbulent Flows - Model Development and Validation", Computers Fluids, 24(3), 227, 1995.
[14] N. P. Siegel, C. K. Ho, S. S. Khalsa and G. J. Kolb, Development and Evaluation of a Prototype Solid Particle Receiver: On-Sun Testing and Model Validation, J Sol Energ-T Asme 132 (2) (2010).
[15] Siegel, N., G. Kolb, K. Kim, V. Rangaswamy, and S. Moujaes, 2007, Solid particle receiver flow characterization studies, Proceedings of the Energy Sustainability Conference 2007, p. 877-883.
[16] Wendelin, T. (2003). "SolTRACE: A New Optical Modeling Tool for Concentrating Solar Optics." Proceedings of the ISEC 2003: International Solar Energy Conference, 15-18 March 2003, Kohala Coast, Hawaii. New York: American Society of Mechanical Engineers, pp. 253-260; NREL Report No. CP-550-32866.
[17] Yellowhair, J., Ho, C. K., "Optical Ray-Tracing Performance Modeling of Quartz Half-Shell Tubes Aperture Cover For Falling Particles Receiver," *Proceedings of the ASME 2019 13th International Conference on Energy Sustainability*, Bellevue, WA, USA, July 15-17, 2019.
[18] Shaeffer, R., Mills, B., Yue, L., Ho, C. K., "Evaluation of Performance Factors for a Multistage Falling Particle Receiver," *to be presented at the 14th International Conference on Energy Sustainability, June 7-11, Denver, CO, USA.*